Elementary Subdomain Technique in Switched Reluctance Machines with the Local Saturation Effect

Mohammed Ben Yahia, Kamel Boughrara, Frédéric Dubas, Lazhar Roubache, Rachid Ibtiouen

Elementary Subdomain Technique in Switched Reluctance Machines with the Local Saturation Effect

Mohammed BEN YAHIA[1], Kamel BOUGHRARA[1], Frédéric DUBAS[2], Lazhar ROUBACHE[3], Rachid IBTIOUEN[1]
[1]Ecole Nationale Polytechnique (LRE-ENP), Rue des Frères Oudek, Hassan Badi, B.P. 182, El-Harrach, 16200, Alger, Algérie.
[2]Département ENERGIE, FEMTO-ST, CNRS, Univ. Bourgogne Franche-Comté, F90000 Belfort, France.
[3]Laboratoire Systèmes Électrotechniques et Environnement (LSEE), Université d'Artois, Béthune, France.

ABSTRACT—The paper's purpose is to present and implement a two-dimensional (2-D) semi-analytical model with the local saturation effect in 6/4 switched reluctance machines (SRM) having a double-layer winding with left and right layer (viz., all teeth wound) supplied by sinusoidal waveform of current (aka, variable flux reluctance machines). It is based on the elementary subdomain (E-SD) technique in polar coordinates by applying the Dubas' superposition technique with the local saturation effect. The model permit to find the magnetic field prediction in all parts of the electrical machine characterized by general solutions to the first three harmonics of magnetostatic Maxwell's equations. In this study, the magnetic flux density distribution inside the SRM, the electromagnetic performances have been calculated and compared with those obtained by the 2-D saturated finite-element (FE) method (FEM). The comparisons with FEM show good results of the proposed approach.

Keywords—Electromagnetic performances; local saturation; switched reluctance machine; elementary subdomain technique.

1. INTRODUCTION

For the past few years, electromagnetic modeling of electrical machines become an interesting axis in the research area. In many electrical engineering applications, this modeling step remains essential to optimize and design electric machines according to specifications. For decades, the numerical methods are widely used in R&D departments for their accuracy as compared to measurement. Nevertheless, mainly in three-dimensional, these approaches are time-consuming and not suitable for the optimization problems. Nowadays, in order to reduce the computation time, hybrid numerical methods can be developed [1]. The actual design works are mainly based on (semi-)analytical methods [2]-[3], viz.,

- equivalent circuits (i.e., electrical, thermal, magnetic…);
- Schwarz-Christoffel mapping method;
- Maxwell-Fourier (i.e., multi-layers models, eigenvalues models, SD technique methods).

Indeed, under certain geometrical and physical assumptions, these techniques have the advantage to be sufficiently explicit/accurate/ fast which make them more flexible as an optimal computer-aided design tool. Currently, the SD technique based on the Maxwell-Fourier method is one of the most used semi-analytical methods. This modeling applied to electrical machines with variable reluctance can be found in [4]-[13], but unfortunately neglecting the global and/or local saturation effect (i.e., the iron parts are considered to be infinitely permeable). In 2017, Dubas *et al.* proposed a new scientific contribution to the SD technique by inserting ferromagnetic regions [2]-[3]. This so-called exact 2-D method has been applied pedagogically to an air- or iron-cored coil supplied by a direct current in Cartesian [2] and polar [3] coordinates. The Dubas' superposition technique has been implemented and applied in radial-flux electrical machines with(out) permanent-magnets supplied by a direct or alternate current (with any waveforms) [14]-[16]. Comparisons with numerical methods give good results. This technique has been extended to:

- the thermal modeling for the steady-state temperature distribution in rotating electrical machines [17];
- E-SD in the rotor and/or stator regions with(out) electrical conductivities for full prediction of magnetic field in rotating electrical machines with the local saturation effect solving by the Newton-Raphson (NR) iterative algorithm [18]-[20].

In this paper, the authors propose to use the E-SD technique in polar coordinates by applying the Dubas' superposition technique to SRM with the local saturation effect, which has not yet been realized in the literature. For example, the scientific contribution has been applied to 6/4 SRM having a double layer winding with left and right layer (viz., all teeth wound) supplied by sinusoidal waveform of current (aka, variable flux reluctance machines). The model permit to find the magnetic field prediction in all parts of the electrical machine characterized by general solutions to the first three harmonics of magnetostatic Maxwell's equations. The proposed E-SD technique is coupled with NR iterative algorithm for nonlinear magnetic field analysis [18]. It is important to note that the developed semi-analytical model is also valid for any number of slot/pole combinations and for non-overlapping teeth wound windings with a single/double layer. Finally, the results of the electromagnetic performances have been performed and validated by the 2-D saturated FEM [21]. The comparisons with FEM show good results of the proposed approach.

2. STUDIED MACHINE AND MAGNETIC FIELD SOLUTIONS

2.1. Machine geometry and assumptions

The studied SRM, as shown on Fig. 1, has been partitioned into 3 regions, both stator and rotor regions are constituted with 5 domains, viz.,

- Region I (air-gap);
- Region II (rotor) contain 2 domains: iron domain Ω_{ri} and the rotor slots domain Ω_{rs} ;
- Region III (stator) contain 3 domains: iron domain Ω_{si} , the coil domain Ω_{ss} and the non-periodic air-gap domain Ω_{sv} (i.e., between the two layers of stator winding).

The semi-analytical model, based on the E-SD technique, is formulated in 2-D, in polar coordinates (r,θ), and in magnetic vector potential $\boldsymbol{A}$ with the following assumptions:

- the end-effects are neglected, i.e., $\boldsymbol{A}=\{0;0;A_z\}$;
- the stator and rotor slots/teeth have radial sides;
- the eddy-current effects in the materials are neglected;
- the current density in the stator slots has only one component along the z-axis, i.e., $\boldsymbol{J}=\{0;0;J_z\}$;
- the magnetic materials are considered as isotropic;
- the iron absolute reluctivity υ is a function of the mean value of magnetic field $\overline{B}$ in each E-SD.

The stator and rotor regions (i.e., Region II and Region III) are meshing in r- and θ-directions into E-SDs as shown in Fig. 2. Each E-SD is characterized by the inner and outer radius, position, opening width, and absolute reluctivity [18]. In this study, the stator/rotor slots/teeth are divided by three in r- and six in θ-direction which give 570 E-SDs in the stator and 288 E-SDs in the rotor. These E-SDs are connected in both directions (i.e., r- and θ-edges) by applying the Dubas' superposition technique. The local saturation effect is solved by the NR iterative algorithm [18].

The general solutions of magnetostatic Maxwell's equations considering only the first three radial and tangential harmonics in each domain Ω can be written as [2]-[3]

$$A_z(r,\theta)=A_z^{\theta}+A_z^{r}+A_{zPi} \tag{1}$$

where

$$A_z^{\theta}=\xi_1+\xi_2\ln(r)+\cdots+\sum_{m=1}^{3}\left[\begin{matrix}\xi_{4m-1}\left(\frac{r}{R_2}\right)^{\delta_n}\\ \cdots+\xi_{4m}\left(\frac{r}{R_1}\right)^{-\delta_n}\end{matrix}\right]\cdot\cos\left[\delta_m\left(\theta-\alpha+\frac{a}{2}\right)\right] \tag{2}$$

$$A_z^{r}=\sum_{m=1}^{3}\left\{\begin{matrix}\xi_{4m+1}\dfrac{\mathrm{sh}\left[\lambda_m\left(\theta-\alpha+\frac{a}{2}\right)\right]}{\mathrm{sh}(\lambda_m a)}\\ \cdots+\xi_{4m+2}\dfrac{\mathrm{sh}\left[\lambda_m\left(\theta-\alpha-\frac{a}{2}\right)\right]}{\mathrm{sh}(\lambda_m a)}\end{matrix}\right\}\cdot\sin\left[\lambda_m\ln\left(\frac{r}{R_1}\right)\right] \tag{3}$$

$$A_{zPi}=\begin{cases}-\mu_0\dfrac{J_{1,2z}^{i}r^2}{4} & \text{if } \Omega\in\Omega_{ss}^{i}\\ 0 & \text{if } \Omega\in\Omega_{ri}\cup\Omega_{rs}^{j}\cup\Omega_{si}\cup\Omega_{sv}\end{cases} \tag{4}$$

where $\delta_m=m\pi/a$ & $\lambda_m=m\pi/\ln(R_2/R_1)$ are the spatial frequency (or periodicity) of A_z^{θ} & A_z^{r} [3]; μ_0 is the vacuum permeability; $J_{1,2z}^{i}$ is the current density for the left (second) and right (first) layer of winding in the i^{th} stator slot with $i=1,\ldots,Q_s$ in which Q_s represents the number of stator slots; Ω_{rs}^{j}, Ω_{ss}^{i}, Ω_{ri}, Ω_{si} and Ω_{sv} are respectively the j^{th} rotor slot, the i^{th} stator slot, the rotor/stator iron and the non-periodic air-gap domains; $\{R_1,R_2,\alpha,a\}$ are the main dimension of Ω; and $\xi_1 \sim \xi_{4m+2}$ are the integration constants (ICs).

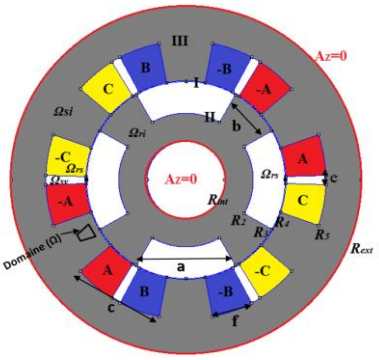

Fig. 1. Studied 6/4 SRM with sinusoidal current excitation having a double-layer winding with left and right layer (viz., all teeth wound).

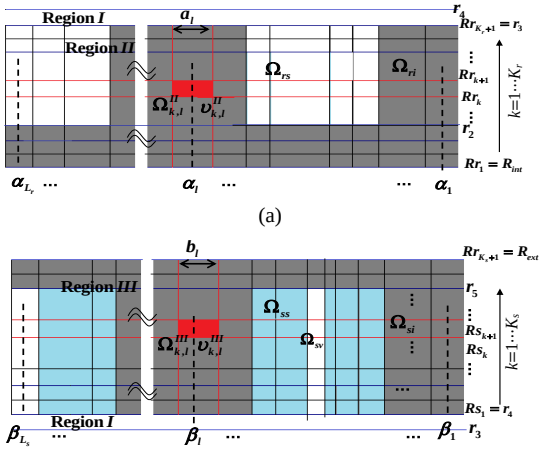

(a)

(b)

Fig. 2. Mesh generation of the: (a) rotor, and (b) stator.

Each E-SD is characterized by absolute reluctivity υ in function of $\overline{B}$ [18]

$$\upsilon(\overline{B})=\frac{1}{\mu_0}\left[1-\frac{Q}{\sum_{q=1}^{Q}\left(\left(\overline{B}/m_q\right)^{n_q}+a_q^{n_q}\right)^{1/n_q}}\right] \tag{5}$$

where q is an index, and $\{m_q,n_q,a_q\}$ are the parameters to be optimized using genetic algorithm. The $B(H)$ and $\upsilon(\overline{B})$ curves used herein are given in [18]. For the domains $\{\Omega_{ss}^{i};\Omega_{rs}^{j};\Omega_{sv}\}$, the absolute reluctivity $\upsilon(\overline{B})=1/\mu_0$.

2.2. *General solution of magnetostatic Maxwell's equations*

2.2.1. *Region I (Air-gap)*

In the air-gap (i.e., Region I), $r\in[R_3;R_4]$ and $\theta\in[0;2\pi]$, the general solution of A_{zI} is defined by:

$$A_{zI}=A1_0+A2_0\ln(r)+\cdots+\sum_{n=1}^{+\infty}\left[\begin{matrix}A1_n\left(\frac{r}{R_s}\right)^{n}+A2_n\left(\frac{r}{R_r}\right)^{-n}\\ \cdots+A3_n\left(\frac{r}{R_s}\right)^{n}+A4_n\left(\frac{r}{R_r}\right)^{-n}\end{matrix}\right]\cdot\begin{matrix}\cos(n\theta)\\ \sin(n\theta)\end{matrix} \tag{6}$$

where n is a positive integer, and $A1_0 \sim A4_n$ are the ICs in Region I.

2.2.2. Region II (Rotor)

The rotor (i.e., Region II) is divided into E-SDs as it shown in Fig. 2(a). Each element $\Omega_{II}^{k,l}$ is characterized by the parameters $\left\{A_{zPII}^{k,l}, \upsilon_{II}^{k,l}, Rr_k, Rr_{k+1}, \alpha_l, a_l\right\}$ where $A_{zPII}^{k,l}$ is the solution particular, $\upsilon_{II}^{k,l}$ is the absolute reluctivity, and $\left\{Rr_k, Rr_{k+1}, \alpha_l, a_l\right\}$ are the corresponding main dimension. The general solution of $A_{zII}^{k,l}$ is similar to (1)~(4) by replacing $\xi_1 \sim \xi_{4m+2}$ with $B_1^{k,l} \sim B_{4m+2}^{k,l}$ and $\left\{R_1, R_2, \alpha, a\right\}$ with $\left\{Rr_k, Rr_{k+1}, \alpha_l, a_l\right\}$.

2.2.3. Region III (Stator)

The stator (i.e., Region III) is divided into E-SDs as it shown in Fig. 2(b). Each element $\Omega_{III}^{k,l}$ is characterized by the parameters $\left\{A_{zPIII}^{k,l}, \upsilon_{III}^{k,l}, Rs_k, Rs_{k+1}, \beta_l, b_l\right\}$ where $A_{zPIII}^{k,l}$ is the particular solution, $\upsilon_{III}^{k,l}$ is the absolute reluctivity and $\left\{Rs_k, Rs_{k+1}, \beta_l, b_l\right\}$ are the corresponding main dimension. The general solution of $A_{zIII}^{k,l}$ is similar to (1)~(4) by replacing $\xi_1 \sim \xi_{4m+2}$ with $C_1^{k,l} \sim C_{4m+2}^{k,l}$ and $\left\{R_1, R_2, \alpha, a\right\}$ with $\left\{Rs_k, Rs_{k+1}, \beta_l, b_l\right\}$.

2.3. Magnetic flux density and electromagnetic source (ES)

2.3.1. Magnetic flux density

The field vectors $\boldsymbol{B} = \left\{B_r; B_\theta; 0\right\}$ and $\boldsymbol{H} = \left\{H_r; H_\theta; 0\right\}$ are coupled by

$$\boldsymbol{H}^{k,l} = \upsilon^{k,l} \cdot \boldsymbol{B}^{k,l}. \tag{7}$$

Using $\boldsymbol{B} = \nabla \times \boldsymbol{A}$, the components of $\boldsymbol{B}$ can be deduced by

$$B_r = \frac{1}{r} \cdot \frac{\partial A_z}{\partial \theta} \text{ and } B_\theta = -\frac{\partial A_z}{\partial r}. \tag{8}$$

2.3.2. ES : Current density in the i^{th} stator slot

The current densities for the left (second) and right (first) layer of winding in the i^{th} stator slot are defined as:

$$J_{1z}^i = \frac{N_c}{S} \cdot C_{(1)}^T \cdot i_g \text{ and } J_{2z}^i = \frac{N_c}{S} \cdot C_{(2)}^T \cdot i_g \tag{9}$$

where $S = f \cdot \left(R_5^{\,2} - R_4^{\,2}\right)/2$ is the surface of the stator slot coil, N_c is the conductors' number of slot coil, $i_g = \left[i_a \quad i_b \quad i_c\right]$ is the vector of phase currents whose currents' waveform is sinusoidal with a phase shift of $2\pi/3$, and $C_{(1)}^T$ & $C_{(2)}^T$ are the transpose of the connecting matrix between the 3-phases current and the stator slots

$$C_{(1)}^T = \begin{bmatrix} -1 & 0 & 0 & 1 & 0 & 0 \\ 0 & 1 & 0 & 0 & -1 & 0 \\ 0 & 0 & -1 & 0 & 0 & 1 \end{bmatrix} \tag{10}$$

$$C_{(2)}^T = \begin{bmatrix} 0 & 0 & -1 & 0 & 0 & 1 \\ -1 & 0 & 0 & 1 & 0 & 0 \\ 0 & 1 & 0 & 0 & -1 & 0 \end{bmatrix}. \tag{11}$$

These connection matrices can be generated automatically by using ANFRACTUS TOOL developed in [22].

3. ICs AND NR ITERATIVE ALGORITHM

From the boundary conditions (BCs) between the various regions, the ICs of 3 regions can be determined by solving the following nonlinear system equations [18]:

$$f(X) = \left[M(X)\right] \cdot X + Y = 0 \tag{12}$$

where

$$M(X) = \begin{bmatrix} \Lambda^{11} & \Lambda^{12} & \Lambda^{13} \\ 0 & \Lambda^{22} & 0 \\ 0 & 0 & \Lambda^{33} \\ \Lambda^{41} & \Lambda^{42}\left(b^{rotor}\right) & \Lambda^{43}\left(c^{stator}\right) \\ 0 & \Lambda^{52}\left(b^{rotor}\right) & 0 \\ 0 & 0 & \Lambda^{63}\left(c^{stator}\right) \end{bmatrix} \tag{13}$$

with

$$X = \left[\mathrm{a}^{air} \quad b^{rotor} \quad c^{stator}\right]^T \tag{14}$$

$$Y = \left[\Gamma^1 \quad \Gamma^2 \quad \Gamma^3 \quad \Gamma^4 \quad \Gamma^5 \quad \Gamma^6\right] \tag{15}$$

$$\mathrm{a}^{air} = \begin{bmatrix} A1_0 \\ \vdots \\ A1_N \\ A2_0 \\ \vdots \\ A2_N \\ A3_1 \\ \vdots \\ A3_N \\ A4_1 \\ \vdots \\ A4_N \end{bmatrix}, \; b^{rotor} = \begin{bmatrix} B_1^{1,1} \\ \vdots \\ B_{4m+2}^{1,1} \\ B_1^{1,2} \\ \vdots \\ B_{4m+2}^{1,2} \\ B_1^{K_r,L_r} \\ \vdots \\ B_{4m+2}^{K_r,L_r} \end{bmatrix} \text{ and } c^{rotor} = \begin{bmatrix} C_1^{1,1} \\ \vdots \\ C_{4m+2}^{1,1} \\ C_1^{1,2} \\ \vdots \\ C_{4m+2}^{1,2} \\ C_1^{K_s,L_s} \\ \vdots \\ C_{4m+2}^{K_s,L_s} \end{bmatrix}. \tag{16}$$

It should be noted that $\left\{\Lambda^{11}; \Lambda^{12}; \Lambda^{13}; \Lambda^{22}; \Lambda^{33}\right\}$ are independent to the absolute reluctivity of materials. However, the other sub-matrices correspond to BCs of $H_{\|}$ at surface, are depending to the absolute reluctivity of materials which are also related the unknowns' vector X. The development of BCs, the various sub-matrices, and the iterative NR algorithm for nonlinear analysis of $\boldsymbol{B}$ by using $B(H)$ curve can be found in [18].

4. RESULTS AND VALIDATIONS

4.1.1. Introduction

The developed model taking into account to the local saturation effect is used to determine the magnetic flux density distribution and the electromagnetic performances of 6/4 SRM with double layer winding. The results of semi-analytic model are verified by 2-D saturated FEM. The magnetic potential vector A_z and flux density $\boldsymbol{B}$ in the various regions have been computed with the finite number of harmonic terms in the air-gap $N_{\max} = 200$ and three harmonics with 288/570 E-SDs in rotor/stator region. For the comparison, the main parameters of the studied machine are given in Table I.

TABLE I. Parameters of 6/4 SRM.

Symbol	Parameter	Value (unit)
Q_s	Number of stator slots	6
Q_r	Number of rotor poles	4
R_2	Internal radius of rotor slot	17.3 (mm)
R_5	External radius of stator slot	36 (mm)
R_{ext}	Radius of the external stator surface	45 (mm)
R_4	Radius of the stator internal surface	25.7 (mm)
R_3	Radius of the rotor surface	26 (mm)
g	Air-gap length	0.2 (mm
L_u	Stack length	60 (mm)
R_1	Radius of the shaft	10 (mm)
a	Rotor slot opening	60 (deg.)
b	Rotor tooth opening	30 (deg.)
c	Stator slot opening	38 (deg.)
d	Stator tooth opening	22 (deg.)
e	Non-periodic air-gap opening	4 (deg.)
f	Opening of a slot coil	17 (deg.)
I_n	Rated phase current	60 (A)
N_c	Conductors' number of slot coil	40
N	Rated speed	1,500 (rpm)

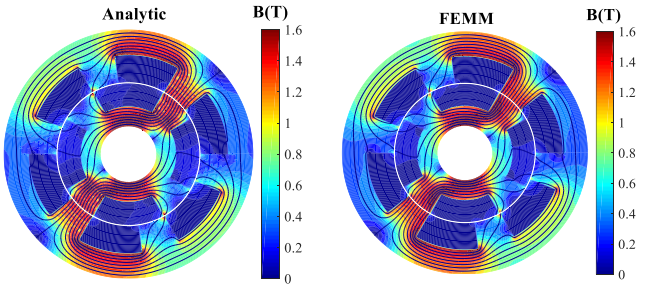

(a) (b)

Fig. 3. Flux density inside the SRM: (a) analytic and (b) FEM.

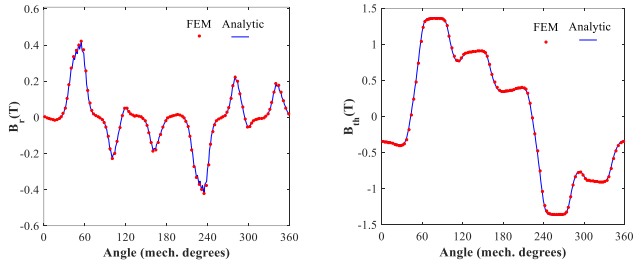

(a) (b)

Fig. 4. Waveform of $\boldsymbol{B}$ in the stator yoke middle at $r=(R_{ext}+R_5)/2$: (a) r- and (b) θ-component.

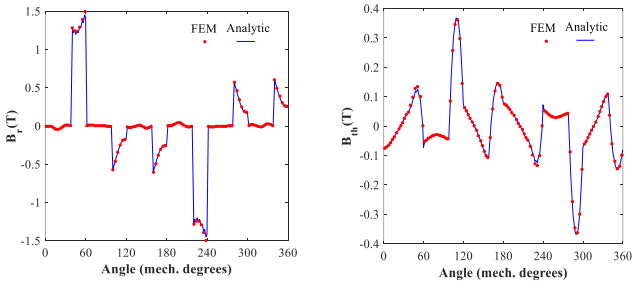

(a) (b)

Fig. 5. Waveform of $\boldsymbol{B}$ in the stator middle at $r=(R_4+R_5)/2$: (a) r- and (b) θ-component.

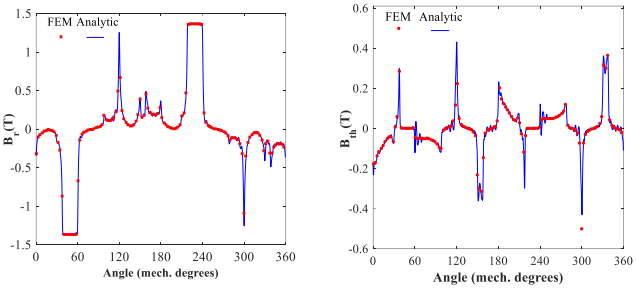

(a) (b)

Fig. 6. Waveform of $\boldsymbol{B}$ in the air-gap middle at $r=(R_3+R_4)/2$: (a) r- and (b) θ-component.

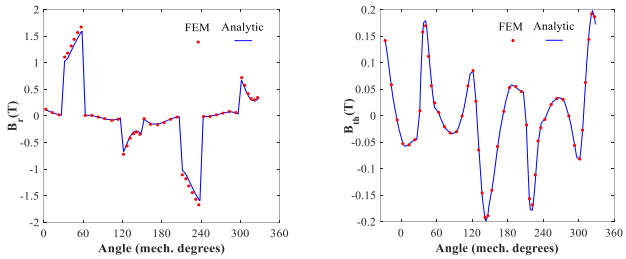

(a) (b)

Fig. 7. Waveform of $\boldsymbol{B}$ in the rotor middle at $r=(R_2+R_3)/2$: (a) r- and (b) θ-component.

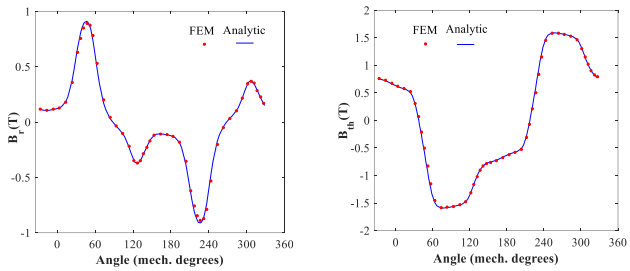

(a) (b)

Fig. 8. Waveform of $\boldsymbol{B}$ in the rotor yoke middle at $r=(R_1+R_2)/2$: (a) r- and (b) θ-component.

4.1.2. *Flux density distribution*

Fig. 3 shows the magnitude of $\boldsymbol{B}$ in all machine's regions for the studied SRM. The comparison between analytical and numerical results improves the model accuracy regarding the local saturation which can be observed in the partial part of stator/rotor yoke and teeth.

In Figs. 4 ~ 8, a numerical and semi-analytical comparison is shown the r- and θ-components of $\boldsymbol{B}$ in the

- stator yoke middle at $r=(R_{ext}+R_5)/2$ (see Fig. 4);
- stator middle at $r=(R_4+R_5)/2$ (see Fig. 5);
- air-gap middle at $r=(R_3+R_4)/2$ (see Fig. 6);
- rotor middle at $r=(R_2+R_3)/2$ (see Fig. 7);
- rotor yoke middle at $r=(R_1+R_2)/2$ (see Fig. 8);

One can see that a very good agreement is obtained for the various components of $\boldsymbol{B}$ in all regions. This confirms that the local saturation effect with the $B(H)$ curve is considered accurately.

4.1.3. *Electromagnetic performances*

Fig. 9 shows the waveform as well as the harmonic spectrum of the static electromagnetic torque which represents

the torque due to a single phase of the electrical machine (e.g., due to phase *A*).

For full-load condition (viz., 60 A@1,500 rpm), the induced magnetic flux linkage per phase is given in Fig. 10.

Fig.12 show the self- and mutual inductance, the simulation is done for nominal current I_n. One can see that the self-inductance is more important in amplitude that the mutual inductance.

All obtained results confirm the accuracy of the proposed semi-analytical model with the local effect saturation considering both amplitude and waveform.

5. Conclusion

In this paper, we have developed a 2-D semi-analytical model for SRM with double-layer winding to predict the magnetic flux density distribution and the electromagnetic performances (viz., the static electromagnetic torque, the magnetic flux linkage, self-/mutual inductances) for any rotor positions. It is based on the exact E-SD technique [18] in polar coordinates by applying the Dubas' superposition technique [2]-[3] with the local saturation effect. It has the ability in any number of stator slots, rotor poles and phases and for different type of stator winding. Because the SRM always operate with certain level of saturation, the proposed model present an accuracy results. It can be considered as a viable alternative to 2-D saturated FEM for analysis of SRM.

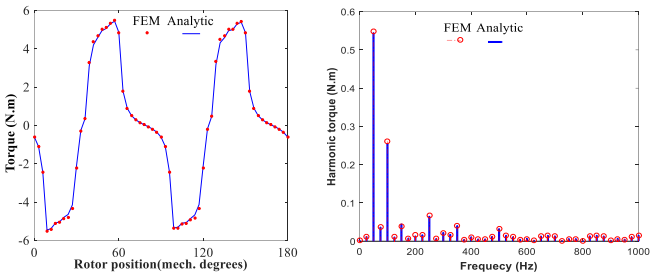

(a) (b)

Fig. 9. The static electromagnetic torque due to phase *A*: (a) waveform, and (b) harmonic spectrum.

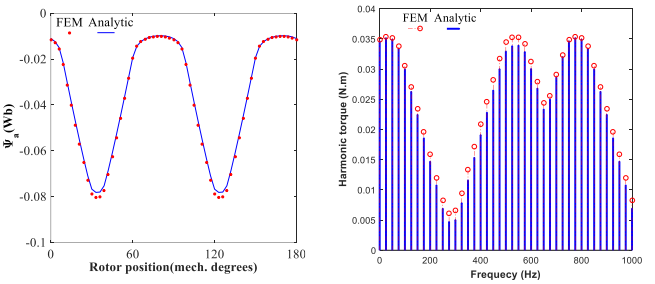

(a) (b)

Fig. 10. The magnetic flux linkage at full-load condition (60 A@1,500 rpm): (a) waveform, and (b) harmonic spectrum.

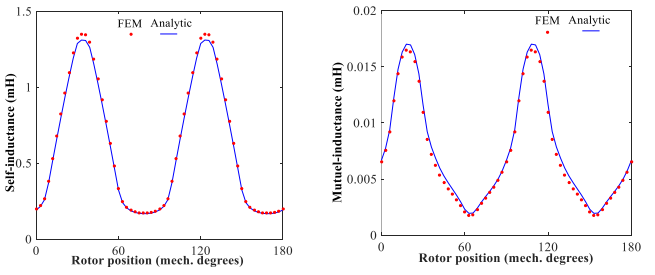

(a) (b)

Fig. 11. Waveform of the: (a) self- and (b) mutual inductance.

6. References

[1] R. Benlamine, F. Dubas, S-A. Randi, D. Lhotellier, and C. Espanet, "3-D numerical hybrid method for PM eddy-current losses calculation: Application to axial-flux PMSMs,". IEEE Trans. Magn., vol. 51, no. 7, Jul. 2017, Art ID 8106110, DOI: 10.1109/TMAG.2015.2405053.

[2] F. Dubas, and K. Boughrara, "New scientific contribution on the 2-D subdomain technique in Cartesian coordinates: Taking into account of iron parts," Math. Comput. Appl., vol. 22, no. 1, p. 17, Feb. 2017, DOI: 10.3390/mca22010017.

[3] F. Dubas, and K. Boughrara, "New scientific contribution on the 2-D subdomain technique in polar coordinates: Taking into account of iron parts," Math. Comput. Appl., vol. 22, no. 4, p. 42, Oct. 2017, DOI: 10.3390/mca22040042.

[4] F. Dubas, and C. Espanet, "Analytical solution of the magnetic field in permanent-magnet motors taking into account slotting effect: No-load vector potential and flux density calculation," IEEE Trans. Magn. vol. 45, no. 5, pp. 2097-2109, May 2009, DOI: 10.1109/TMAG.2009.2013245.

[5] E. Devillers, J. Le Besnerais, T. Lubin, M. Hecquet, and J.P. Lecointe, "A review of subdomain modeling techniques in electrical machines: Performances and applications," *in Proc.* ICEM, Lausanne, Switzerland, 04-07 Sep., 2016, DOI: 10.1109/ICELMACH.2016.7732510.

[6] H. Tiegna, Y.Amara, and G. Barakat, "Overview of analytical models of permanent magnet electrical machines for analysis and design purposes," Mathematics and Computers in Simulation, vol. 90, pp. 162-177, Apr. 2013, DOI: 10.1016/j.matcom.2012.12.002.

[7] K. Boughrara, T. Lubin, and R. Ibtiouen, "General subdomain model for predicting magnetic field in internal and external rotor multiphase flux-switching machines topologies," IEEE Trans. Magn., vol. 49, no. 10, pp. 5310-5325, Oct. 2013, DOI: 10.1109/TMAG.2013.2260827.

[8] M. Curti, J.J.H. Paulides, and E.A. Lomonova, "An overview of analytical methods for magnetic field computation," *in Proc.* EVER, Grimaldi Forum, Monaco, 31 Mar./02 Apr., 2015, DOI: 10.1109/EVER.2015.7112938.

[9] F. Dubas, and A. Rahideh, "A 2-D analytical PM eddy-current loss calculations in slotless PMSM equipped with surface-inset magnets," IEEE Trans. Magn., vol. 50, no. 3, Mar. 2014, Art. ID 6300320, DOI: 10.1109/TMAG.2013.2285525.

[10] K. Boughrara, F. Dubas, and R. Ibtiouen, "2-D analytical prediction of eddy currents, circuit model parameters, and steady-state performances in solid rotor induction motors," IEEE Trans. Magn., vol. 50, no. 12, Dec. 2014, Art. ID 7028214, DOI: 10.1109/TMAG.2014.232666.

[11] K. Boughrara, N. Takorabet, R. Ibtiouen, O. Touhami, and F. Dubas, "Analytical analysis of cage rotor induction motors in healthy, defective, and broken bars conditions," IEEE Trans. Magn., vol. 51, no. 2, Feb. 2015, Art. ID 8200317, DOI: 10.1109/TMAG.2014.2349480.

[12] L. Roubache, K. Boughrara, and R. Ibtiouen, "Analytical electromagnetic analysis of multi-phases cage rotor induction motors in healthy, broken bars and open phases conditions," Progress In Electromagnetics Research B, vol. 70, pp. 113-130, Oct. 2016, DOI: 10.2528/PIERB16072510.

[13] F. Chen, C. Zhang, J. Chen, and G. Yang, "Accurate subdomain model for computation magnetic field of short moving-magnet linear motor with Halbach array," IEEE Trans. Magn., vol. 56, no. 9, Art ID 8200509, DOI: 10.1109/TMAG.2020.3002457.

[14] L. Roubache, K. Boughrara, F. Dubas, and R. Ibtiouen, "New subdomain technique for electromagnetic performances calculation in radial-flux electrical machines considering finite soft-magnetic material permeability," IEEE Trans. Magn., vol. 54, no. 4, Art. ID 8103315, Apr. 2018, DOI: 10.1109/TMAG.2017.2785254.

[15] M. Ben Yahia, L. Roubache, Z.K. Djelloul, K. Boughrara, F. Dubas, and R. Ibtiouen, "A 2-D exact subdomain technique in switched reluctance machines taking into account of finite soft-magnetic material permeability," *in Proc.* CISTEM, Algiers, Algeria, 28-31 Oct., 2018, DOI: 10.1109/CISTEM.2018.8613599.

[16] M. Ben Yahia, K. Boughrara, F. Dubas, L. Roubache, and R. Ibtiouen, "Two-dimensional exact subdomain technique of switched reluctance Machines with sinusoidal current excitation," Math. Comput. Appl., vol. 23, no. 4, p. 59, Oct. 2018, DOI: 10.3390/mca23040059.

[17] K. Boughrara, F. Dubas, and R. Ibtiouen, "2-D exact analytical method for steady-state heat transfer prediction in rotating electrical machines,"

IEEE Trans. Magn., vol. 54, no. 9, Art. ID 8104519, Sep. 2018, DOI: 10.1109/TMAG.2018.2851212.

[18] L. Roubache, K. Boughrara, F. Dubas, and R. Ibtiouen, "Elementary subdomain technique for magnetic field calculation in rotating electrical machines with local saturation effect," COMPEL - Int. J. Comput. Math. Electr. Electron. Eng., vol. 38, no. 1, pp. 24-45, Jan. 2019, DOI: 10.1108/COMPEL-11-2017-0481.

[19] L. Roubache, K. Boughrara, F. Dubas, and R. Ibtinouen, "Technique en sous-domaines élémentaires dans les machines asynchrones à cage d'écureuil : Saturation magnétique locale & Courants de Foucault dans les barres," *in Proc.* SGE, Nancy, France, 3-5 Juillet 2018.

[20] L. Roubache, M. Ben Yahia, K. Boughrara, F. Dubas, and R. Ibtiouen, "Analytical modelling of electromagnetic noise in spoke-type permanent-magnet machines," *in Proc.* CISTEM, Algiers, Algeria, 28-31 Oct., 2018, DOI: 10.1109/CISTEM.2018.8613422.

[21] D.C. Meeker, "Finite Element Method Magnetics," Ver. 4.2., Available online: www.femm.info/wiki/download (accessed on 10 October 2018).

[22] D. Ouamara, F. Dubas, M.N. Benallal, S-A. Randi, and C. Espanet, "Automatic winding generation using matrix representation - ANFRACTUS Tool 1.0 -,"Acta Polytechnica, vol. 58, no. 1, pp. 37-46, Mar. 2018, DOI: 10.14311/AP.2018.58.0037.